

# **Gabor depth imaging using a new adaptive partitioning algorithm**

Yongwang Ma and Gary F. Margrave

## **ABSTRACT**

Wavefield extrapolation by spatially variable phase shift is currently a very competitive depth migration technique. In this paper, we present prestack migration results of the Marmousi synthetic dataset using a new adaptive Gabor wavefield extrapolation.

Gabor depth imaging algorithm can be used to approximate the generalized phase-shift-plus-interpolation or the non-stationary phase shift, which are two extreme cases in Gabor imaging schemes. Therefore, there are many ways to explore wavefield extrapolations with Gabor imaging method. The key to an efficient Gabor imaging algorithm is to develop an adaptive partitioning scheme that only localizes the wavefield as required by the lateral velocity variation. We have tested three methods of adaptive partitioning, however, those two presented previously have their limits and they are relatively more difficult to implement in 2D (for 3D imaging) than the one we will describe. We present the details of the new adaptive partitioning method in 1D (for 2D imaging). The extension of the partitioning method to 2D will be described in another paper in this volume. This method creates adaptive partitions using a controlled lateral position error. Software has been developed using the new adaptive partitioning algorithm, reducing substantially computation burden in depth imaging when compared to the full generalized phase-shift-plus-interpolation integral. The performance of Gabor depth imaging using this adaptive partitioning algorithm is illustrated with images from prestack depth migration of the Marmousi dataset.

## **INTRODUCTION**

Migration with phase shift (Gazdag, 1978) (also referred to as wavefield extrapolation with phase shift) was proposed for accurate and efficient depth imaging over other wave-equation migration methods such as those using the finite difference algorithm (e.g. Claerbout and Doherty, 1972; Loewenthal et al., 1976). An important property of phase-shift wavefield extrapolation is its unconditional stability, and it is easy to extend to higher dimensions (e.g., 3D) (Gazdag and Sguazzero, 1984). However, this is not always the case for other wave-equation migration methods. Phase-shift wavefield extrapolation shows its promising features in migrating seismic data, especially in 3D due to its accuracy, speed and relative simplicity. One drawback for the Gazdag (1978) phase-shift method is its assumption of uniform lateral velocity structures, which is not desirable in many practical cases. In the real world, velocity structures are mostly heterogeneous with strong velocity fluctuations in the lateral dimensions, making it undesirable to use the phase-shift method. To address the problem, phase shift plus interpolation (PSPI) was invented (Gazdag and Sguazzero, 1984). PSPI method is implemented by use of a set of reference (laterally homogeneous) velocities to compute extrapolated wavefields; the final wavefield extrapolation is obtained by interpolating with velocities corresponding to certain lateral positions. Kosloff and Kessler (1987) came up with a generalized phase-shift (GPS) to extend the phase-shift method to arbitrary velocity structures using an eigenvalue decomposition tech-

nique. Stoffa et al. (1990) used an alternative wavefield extrapolation algorithm, split-step Fourier migration, dealing with lateral velocity variation while keeping the advantages of the phase-shift method, i.e., accuracy and efficiency. Other phase-shift wavefield extrapolation methods such as ‘phase-screen propagator’ (Wu and Huang, 1992; Roberts et al., 1997; Rousseau and de Hoop, 2001; Jin et al., 2002) are also provided for accurate imaging of abrupt velocity variations in such geological settings as salt-dome environments. The generalized phase-shift (GPS) method and the split-step Fourier method compute thin-lens phase delay (related to velocity variations) in the space-frequency domain and calculate phase-shift due to velocity perturbations in the frequency-wavenumber domain. Jin and Wu (1998) tested windowed phase-screen propagators and showed improved results of depth imaging compared to those from old phase-screen methods. Margrave and Ferguson (1999); Ferguson and Margrave (2002) used a non-stationary phase shift (NSPS) method and a generalized phase shift plus interpolation (GPSPI) to improve migration results, where wavefield extrapolations were done totally in the Fourier domain using exact velocity variations.

Gabor imaging method is related to the method of Jin and Wu (1998) and it approximates GPSPI with a Gabor extrapolator. To reduce the redundancy of computation, we applied adaptive partitioning methods using lateral velocity gradients (Grossman et al., 2002a,b; Ma and Margrave, 2005b, 2006c) and the phase errors between the GPSPI and the Gabor extrapolators (Ma and Margrave, 2006b). However, in this paper we introduce a new adaptive partitioning algorithm depending on the lateral position error criterion. The new adaptive partitioning method is less difficult to extend from 1D partitioning to 2D partitioning.

In the following sections, details of the adaptive Gabor wavefield extrapolation algorithms will be shown.

## **GABOR WAVEFIELD EXTRAPOLATION THEORY**

### **Wavefield extrapolation using GPSPI**

Gabor wavefield extrapolation theory was previously described by Grossman et al. (e.g. 2002a,b) and Ma and Margrave (e.g. 2005b). However, we would like to interpret it in a different way, trying to make it more understandable for general readers.

The following convention are used in this paper for the forward and inverse Fourier transforms, which are

$$\hat{u}(k_x) = \int_{\mathbb{R}} u(x) \exp(ik_x x) dx, \quad (1)$$

and

$$u(x) = \frac{1}{2\pi} \int_{\mathbb{R}} \hat{u}(k_x) \exp(-ik_x x) dk_x, \quad (2)$$

where  $\hat{u}$  is the Fourier spectrum of  $u$ ,  $\mathbb{R}$  is the real domain for integrations,  $k_x$  is the coordinate in the Fourier domain. In the following sections,  $F$  and  $F^{-1}$  will be used to symbolize the forward and inverse Fourier transforms, respectively.

The generalized phase shift plus interpolation (GPSPI) is formulated as (Margrave and Ferguson, 1999; Margrave et al., 2004, 2006)

$$\psi_P(x, z + \Delta z, \omega) = \frac{1}{2\pi} \int_{\mathbb{R}} \hat{\psi}(k_x, z, \omega) \hat{W}(k(x), k_x, \Delta z) \exp(-ik_x x) dk_x, \quad (3)$$

where  $x$  denotes transverse coordinates,  $\hat{\psi}(k_x, z, \omega)$  is the Fourier spectrum (FK) of  $\psi(x, z, t)$ ,  $k_x$  is called the transverse wavenumber,  $k_x$  and  $k_z$  (to be defined in the following) compose the total wavenumber vector with a magnitude of  $k(x)$ ,  $\Delta z$  is the step size of extrapolation in  $z$  (vertical) direction,  $\omega$  is temporal angular frequency and  $v(x)$  denotes the lateral velocity at  $x$  along a slab with thickness  $\Delta z$ . Equation (3) extrapolates wavefields at depth  $z$  down to depth  $z + \Delta z$  in the frequency-wavenumber domain and transforms them into the frequency-space domain using the inverse Fourier transform.  $\hat{W}$  is called the GPSPI wavefield extrapolator, which is a spatial phase shift term and defined as

$$\hat{W}(k(x), k_x, \Delta z) = \exp(ik_z(k(x), k_x) \Delta z), \quad (4)$$

$$k_z(k(x), k_x) = \begin{cases} \sqrt{k^2(x) - k_x^2}, & k^2(x) > k_x^2 \\ i\sqrt{k_x^2 - k^2(x)}, & k^2(x) < k_x^2. \end{cases} \quad (5)$$

and

$$k(x) = \frac{\omega}{v(x)}. \quad (6)$$

Using the convention and symbols for the Fourier transform, equation (3) is written as

$$\psi_P(x, z + \Delta z, \omega) = F^{-1} \left[ \hat{W}(k(x), k_x, \Delta z) F\psi(x, z, \omega) \right]. \quad (7)$$

### Approximation of GPSPI

The GPSPI extrapolator is approximated using

$$\hat{W}(k(x), k_x, \Delta z) \approx \sum_{j \in \mathbb{Z}} \Omega_j(x) S_j(x) \hat{W}(k_j, k_x, \Delta z), \quad (8)$$

where  $\Omega_j$  is a set of windows forming a partition of unity (POU), which means

$$\sum_{j \in \mathbb{Z}} \Omega_j(x) = 1, \quad (9)$$

where  $\mathbb{Z}$  denotes the integer set. The split-step Fourier operator is defined as

$$S_j(x) = \exp \left( i\omega \Delta z \left( \frac{1}{v(x)} - \frac{1}{v_j} \right) \right) \quad (10)$$

and  $\hat{W}(k_j, k_x, \Delta z)$  is a locally constant wavefield extrapolator (refer to equations (4) and (5)) related to  $k_j$  and reference velocities  $v_j$  defined as

$$k_j = \frac{\omega}{v_j} \quad (11)$$

and

$$v_j = \frac{\int_{\mathbb{R}} \Omega_j(x) v(x) dx}{\int_{\mathbb{R}} \Omega_j(x) dx}. \quad (12)$$

Using approximation in equation (8), GPSPI formula (3) can be written as

$$\psi_P(x, z + \Delta z, \omega) \approx \sum_{j \in \mathbb{Z}} \Omega_j(x) S_j(x) \int_{\mathbb{R}} \hat{\psi}(k_x, z, \omega) \hat{W}(k_j, k_x, \Delta z) \exp(-ik_x x) dk_x \quad (13)$$

where  $\Omega_j(x)$  and  $S_j(x)$  are  $k_x$  independent and taken out of the integrand. Using the Fourier symbols in equation (13) gives

$$\psi_P(x, z + \Delta z, \omega) \approx \sum_{j \in \mathbb{Z}} \Omega_j(x) S_j(x) F^{-1} \left[ \hat{W}(k_j, k_x, \Delta z) F \psi(x, z, \omega) \right]. \quad (14)$$

### Gabor Wavefield Extrapolation

To relate equation (13) to Gabor wavefield extrapolation, the Gabor transform should be introduced. Starting with the partition of unity (see equation (9)), one can decompose  $\Omega_j(x)$  as (Grossman et al., 2002a)

$$g_j(x) = \Omega_j^p(x), \quad \gamma_j(x) = \Omega_j^{1-p}(x), \quad p \in [0, 1] \quad (15)$$

where  $g_j(x)$  and  $\gamma_j(x)$  are called analysis and synthesis windows, respectively. The forward Gabor transform is defined as

$$V_g \left( j, \hat{\psi}(k_x) \right) = F [g_j(x)\psi(x)], j \in \mathbb{Z} \quad (16)$$

where  $V_g \left( j, \hat{\psi}(k_x) \right)$  is called the Gabor spectrum of  $\psi(x)$ .  $V_g \left( j, \hat{\psi}(k_x) \right)$  is actually a series of Fourier transforms of the input signal  $\psi(x)$  windowed by  $g_j(x)$ , and it can be recovered by the inverse Gabor transform

$$\psi(x) = V_\gamma^{-1} [V_g(j, \psi(x))] = \sum_{j \in \mathbb{Z}} \gamma_j(x) F^{-1} F [g_j(x)\psi(x)], \quad (17)$$

where  $V_\gamma^{-1}$  stands for the inverse Gabor transform, the inverse Fourier transform on the Gabor spectrum (windowed Fourier spectra) and summation over windows  $\gamma_j(x)$ .

Since  $F^{-1}F = 1$ , proof of equation (17) is immediate using equations (9) and (15) in equation (17).

Since  $p \in [0, 1]$ , we have infinitely many ways to choose the Gabor transform. If we choose  $p = 0$  in equation (15), then we have

$$g_j(x) = 1, \gamma_j(x) = \Omega_j(x). \quad (18)$$

Using equation (18) in equation (17) gives

$$\psi(x) = V_\gamma^{-1} [V_g(j, \psi(x))] = \sum_{j \in \mathbb{Z}} \Omega_j(x) F^{-1} F [\psi(x)]. \quad (19)$$

Equation (19) does nothing but transform  $\psi(x)$  back and forth to the Gabor domain. If we insert a wavefield extrapolator  $\hat{W}(k_j, k_x, \Delta z)$  and  $S_j(x)$  in front of  $F$  and  $F^{-1}$ , respectively, in equation (19), we have exactly equation (14). That is why equation (14) is called the Gabor wavefield extrapolation; it is just one of those cases ( $p$  values) in Gabor extrapolation schemes, an extreme case with  $p = 0$ . Equation (14) is the formula used as the Gabor wavefield extrapolation approximating GPSPI in the following sections.

### Building Adaptive Partitions

Equation (8), i.e.

$$\hat{W}(k(x), k_x, \Delta z) \approx \sum_{j \in \mathbb{Z}} \Omega_j(x) S_j(x) \hat{W}(k_j, k_x, \Delta z), \quad (20)$$

indicates that originally  $\Omega_j(x_x)$  refers to a set of narrow windows uniformly distributed along the  $x$  coordinate. However, to calculate efficiently, we should reduce the number of windows to as few as possible without sacrificing accuracy. This can be done by adaptive partitioning algorithms, where the number of partitions is related to lateral velocity variations. There are several methods (Grossman et al., 2002a,b; Ma and Margrave, 2005a) available. In this paper, a new scheme is proposed for adaptive partitioning in Gabor wavefield extrapolation, which uses “lateral position error” as a criterion.

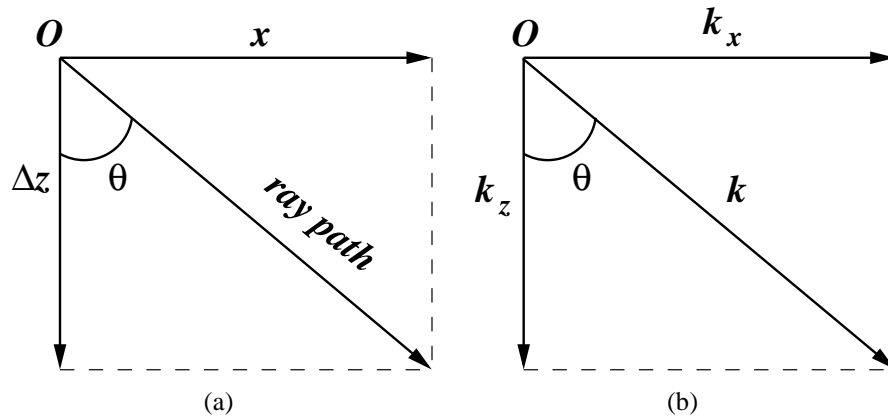


FIG. 1. Geometrical relationships of a local ray path between the vertical and lateral components in the spatial (a) and wavenumber (b) domains.

Starting from a ray path of local scattering wavefield at  $O$  (see Figure 1 (a)), we can write

$$x = \Delta z \tan \theta, \quad (21)$$

where  $x$  is the lateral coordinate,  $\Delta z$  is the extrapolation step size, and  $\theta$  is a scattering angle at this point. Similarly, there is a geometry relationship between the  $k_x$ ,  $\theta$  and  $k(x)$  (see Figure 1 (b)), i.e.,

$$k = \frac{k_x}{\sin \theta} = \frac{\omega}{v}, \quad (22)$$

where  $k_x$  is the transverse wavenumber, and  $k$  denotes the total wavenumber.

Differentiating on both sides of equation (21) and equation (22) and rearranging gives

$$\delta x = \Delta z \sec^2 \theta \frac{\partial \theta}{\partial v} \delta v \quad (23)$$

and

$$\frac{\partial \theta}{\partial v} = \frac{k_x}{\omega} \sec \theta. \quad (24)$$

Substituting equation (24) into equation (23) and simplifying yields

$$\delta v = \frac{\cos^3 \theta}{\sin \theta} \frac{\delta x}{\Delta z} v. \quad (25)$$

Equation (25) shows the way of estimating the velocity variation  $\delta v$  with respect to certain velocity  $v$  given  $\Delta z$ ,  $\theta$  and lateral position error  $\delta x$ . This is the key formula of choosing reference velocities for adaptive Gabor wavefield extrapolation.

To specify reference velocities,  $v_1$  is chosen as the most frequently occurring velocity (easily done from a histogram of the discretely sampled  $v(x)$ ) and then  $\delta v_1$  is obtained from equation (25) as  $\delta v_1 = a v_1$ , where  $a = (\cos^3 \theta \sin^{-1} \theta \delta x / \Delta z)$ . Letting  $v_2$  denote the next higher reference velocity and  $v_3$  the next lower, we set the conditions

$$v_1 - \frac{1}{2} \delta v_1 = v_3 + \frac{1}{2} \delta v_3 = v_3 \left(1 + \frac{1}{2} a\right) \quad (26)$$

and

$$v_1 + \frac{1}{2} \delta v_1 = v_2 - \frac{1}{2} \delta v_2 = v_2 \left(1 - \frac{1}{2} a\right). \quad (27)$$

Using (26) and (27), calculation of  $v_2$  and  $v_3$  is obvious, giving

$$v_2 = \frac{2v_1 + \delta v_1}{2 - a} \quad (28)$$

and

$$v_3 = \frac{2v_1 - \delta v_1}{2 + a}. \quad (29)$$

Proceeding in a similar way until a reference velocity exceeds the range of  $v(x)$ , which defines a complete set of reference velocities. The use of equation (25) in selecting distance between reference velocities suggests that lateral position error will be bounded by  $\delta x$ . This bound may not be strictly held because equation (25) was derived with constant velocity theory; however, it should still be a good constraint.

Once the reference velocities are selected, they can be used as measures (see Figure 2 (b)) to build indicator functions  $I_j(x)$  using

$$I_j(x) = \begin{cases} 1, & |v(x) - v_j| = \min \\ 0, & \text{otherwise,} \end{cases} \quad (30)$$

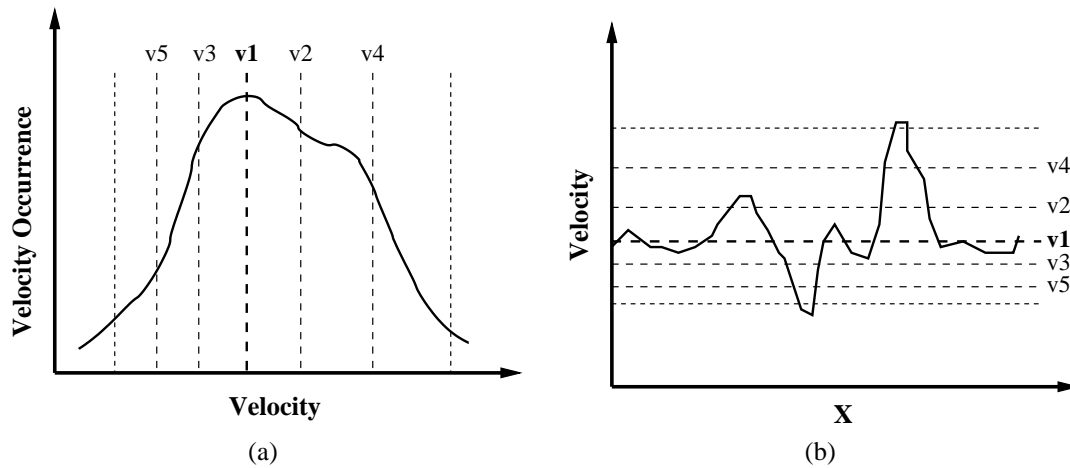


FIG. 2. Build indicator functions (a table) using the adaptive partitioning algorithm given a certain lateral position error. In (a), we find the reference velocities according to a certain lateral position error criterion (see equation (25)); the solid curve indicates occurrences of velocities; the dashed lines (vertical) correspond to the reference velocity values selected by the adaptive partitioning algorithm. In (b), we build indicator functions using exact velocity (profile) values and the reference velocities selected in (a) (see equation (30)); the solid curve shows the velocity profile; dashed lines (horizontal) are reference velocities created in (a).

where  $v(x)$  is the exact velocity at the lateral position  $x$  and  $v_j$  ( $j = 1, 2, \dots, n$ ) are reference velocities created by equation (25).

We convolve the indicator function  $I_j$  with a unit window (atomic window) to create partitioning windows (forming a POU) corresponding to reference velocities used in Gabor wavefield extrapolation. This is done by

$$\Omega_j(x) = (I_j * \Theta)(x), \quad (31)$$

where  $\Theta$  is the atomic window. The atomic window can be any type of window, such as the Gaussian window, with localization property;  $*$  means normalized convolution.

For 2D wavefield extrapolation, the partitioning scheme works in 1D; and this method can be easily extended to 2D partitioning required for 3D Gabor wavefield extrapolation (Ma and Margrave, 2006a).

To show how the adaptive partitioning method works, a few partitioning examples are shown. In the first example, the adaptive partitioning method was applied to a simple step velocity model. Given a lateral position error criterion, the algorithm chooses to create two windows corresponding to two distinct velocity segments (see Figure 3 (a)), which is expected.

The second velocity model is a bump velocity function (see Figure 3 (b)); two velocity segments on both sides of the bump have the same velocity value. The adaptive partitioning algorithm chooses two windows according to a given lateral position error. The green window (dashed line) goes in from the left side, goes out and comes back again on the right side, corresponding to one reference velocity; the blue window (solid line) follows

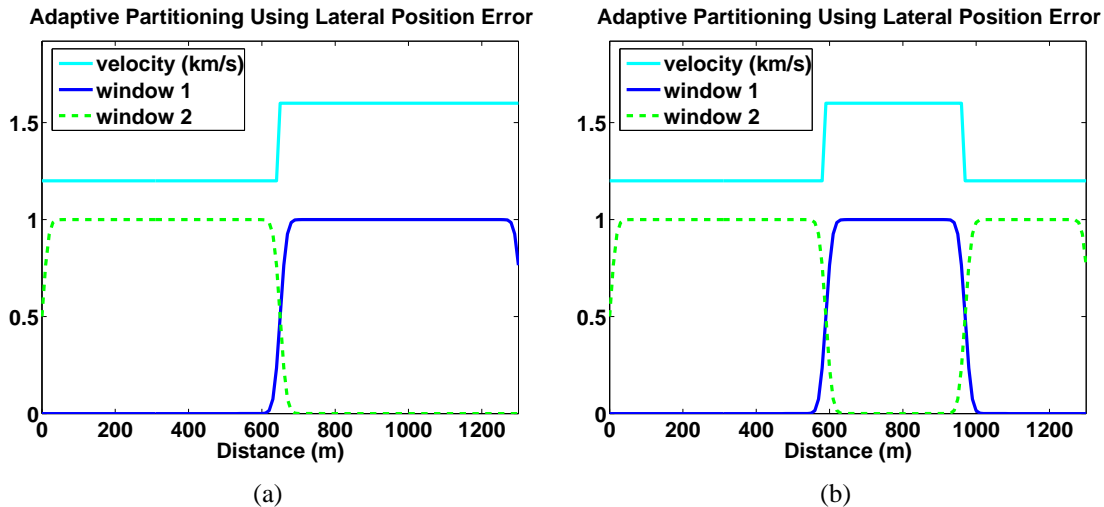


FIG. 3. Adaptive partitioning examples: In (a) a step velocity profile (shown in cyan colour) is used to test adaptive partitioning algorithm. We see two windows (one in green-dashed line and the other in blue-solid line) created using a certain lateral position criterion; in (b), a bump velocity profile (shown in cyan colour) is used, since we set the velocity on both sides of the bump the same value, two reference velocity is selected by the adaptive partitioning algorithm. As a result, we have two windows by the algorithm given a lateral position error criterion.

the constant velocity segment in the center portion. It is also shown that the partitioning result of a velocity profile consisting of several kinds of velocity segments (see Figure 4). This shows the new adaptive partitioning algorithm is able to deal with such complicated lateral velocity variations as those in the Marmousi velocity model.

## GABOR IMAGING EXAMPLES

The Marmousi synthetic dataset has been widely used as a benchmark for testing depth imaging algorithms. The Marmousi velocity section used in Gabor depth imaging in this paper is shown in Figure 5 (a). In the Marmousi synthetic dataset, there are 240 shot records with a recording time of about 2.9 seconds. All depth migrations using the adaptive Gabor imaging method have been done using prestack shot records, each of which includes 241 extrapolation steps with step size of  $\Delta z = 12.5$  meters.

Figure 5 (b) shows the Gabor imaging result of the Marmousi dataset using a position error of 5 m as criterion in the adaptive partitioning. Taking a closer look at the imaging target (a reservoir extending from distance 6000 m to 7500 m in depth about 2500 m, see also Figure 5 (a)), we know that the target reservoir has been accurately imaged (compare this portion in the image to the corresponding part in the original velocity structures). Observing the rest of the areas in the Marmousi image (Figure 5 (a) and (b)), we see that they are all well imaged using the Gabor migration method.

We would like to push the Gabor (approximating GPSPI) imaging method a bit more in the accuracy direction, i.e., a smaller position criterion, 2.5 m, was used. Figure 5 (c) shows the result of this application. Comparing carefully to the imaging result using 5 m position error, it can be seen that there is improvement throughout the section, especially the fault

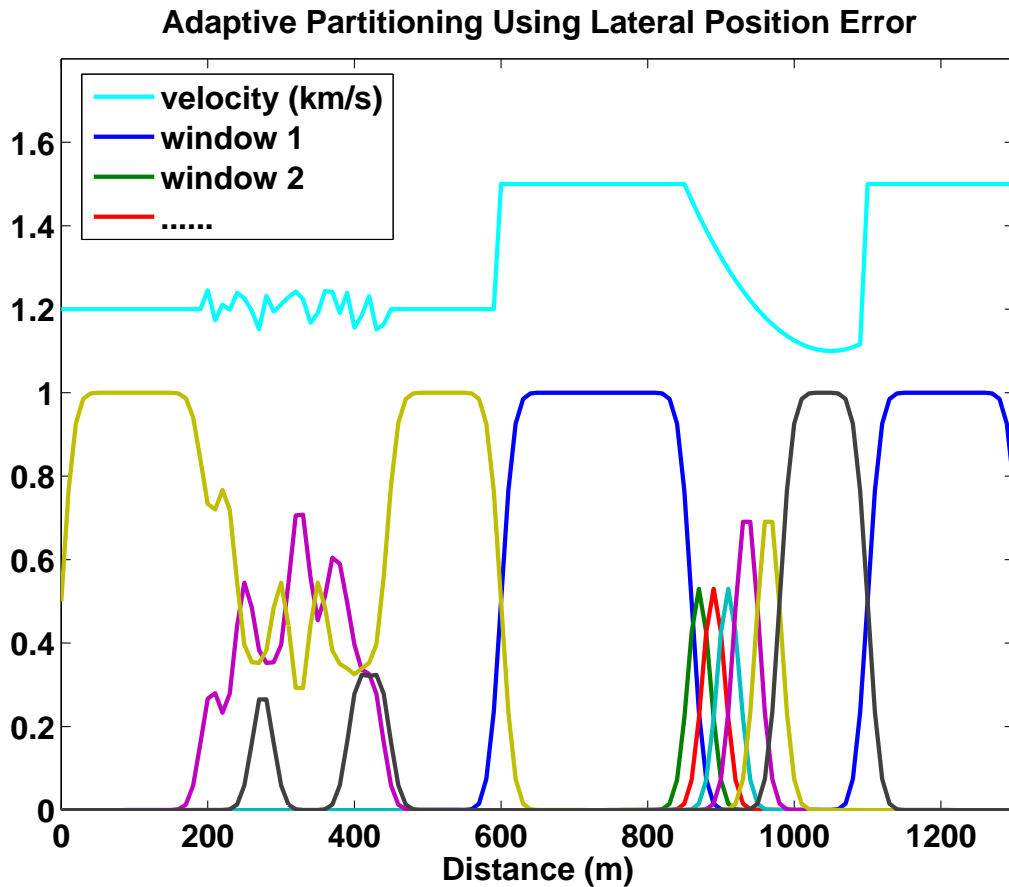


FIG. 4. Adaptive partitioning on a complex velocity model. A specific colour shows a single partition created by the adaptive partitioning algorithm. It can be seen that at some positions there is overlapping of different partitions, which indicates implicit interpolations in Gabor depth imaging when windowing the wavefield to be extrapolated with such partitions.

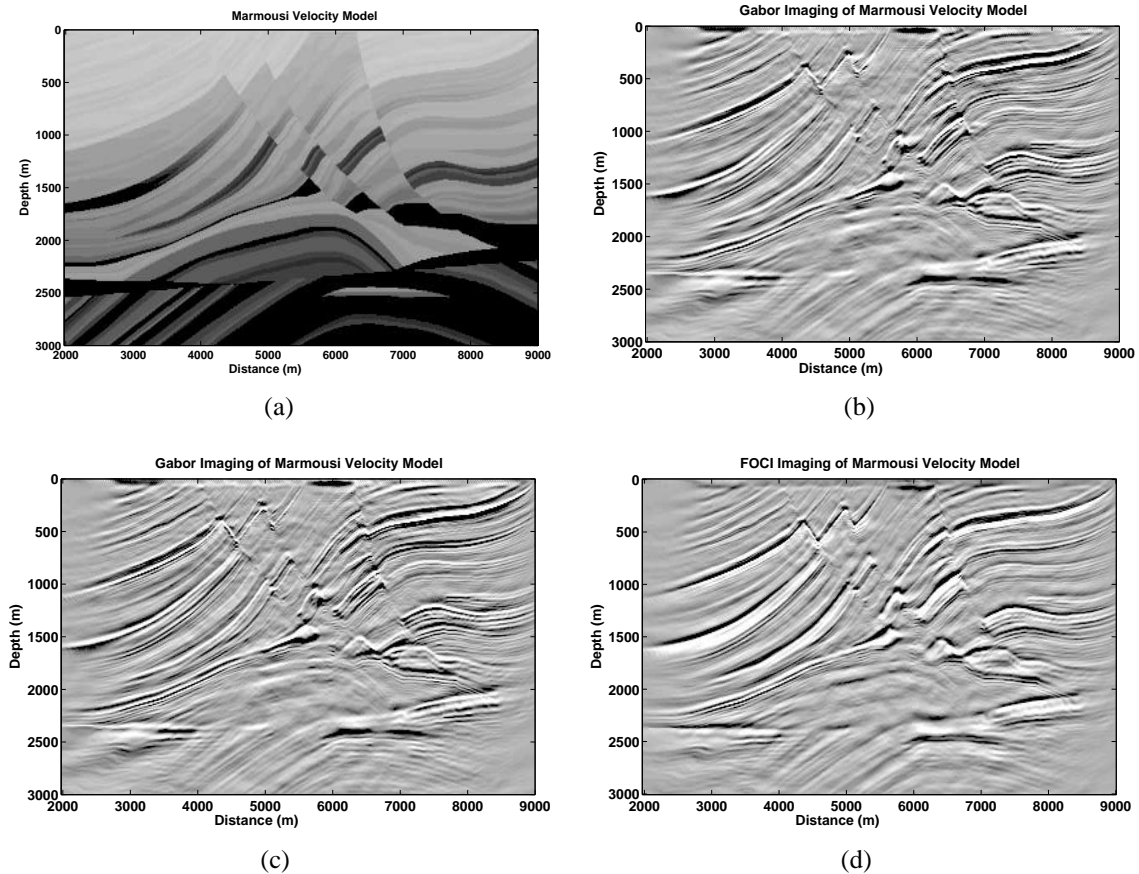


FIG. 5. Marmousi velocity structures and the imaging results using the Gabor and FOCI methods. (a) Marmousi velocity structures used in the imaging. (b) Gabor imaging result using a lateral position error of 5 m. (c) Gabor imaging result using a lateral position error of 2.5 m. (d) FOCI imaging result using an operator of 51 points (Margrave et al., 2006).

areas in the shallow middle part. However, it can also be noticed that the improvement of the reservoir image is slight. We say that 5 m criterion may be good enough for the target imaging if the running time is more important than the high resolution images. Using 2.5 m position error in the Gabor imaging consumes about another 50% running time compared to the one using 5 m position error.

Another merit of the Gabor imaging method is shown by competitively high resolution images. We compared the Gabor imaging result to that of a known excellent imaging tool FOCI (Margrave et al., 2004, 2006) (see Figure 5 (d)). The images for comparison are the best images of the two methods consuming comparable running time (see Figure 5 (c) and (d)). The close-ups from both images in the upper middle part are shown to tell the difference between them; these zoomed-in parts are fault zones in the upper-middle portions of the Marmousi images (see Figure 6 (a) and Figure 6 (b)). From visual observation, we conclude that the Gabor imaging method gives a better resolution than FOCI.

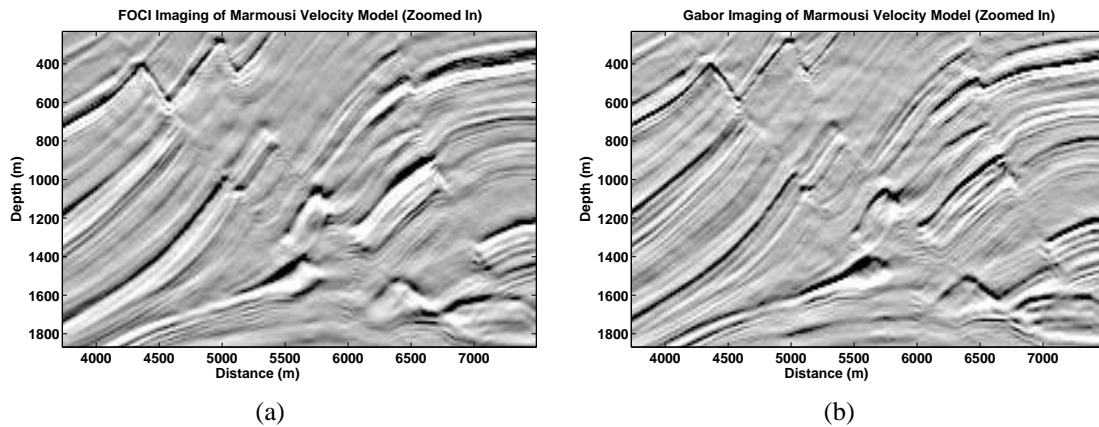


FIG. 6. A detailed comparison between the Marmousi imaging using the FOCI and Gabor methods. (a) FOCI imaging enlargement. (b) Gabor imaging enlargement.

## CONCLUSIONS AND DISCUSSIONS

The approximation of GPSPI using the adaptive Gabor wavefield extrapolation algorithm has shown itself to be a very good and promising depth imaging method. The adaptive partitioning algorithm helps to achieve efficient depth imaging and the imaging accuracy and speed can be controlled using the adaptive partitioning scheme.

There are still many aspects in the Gabor imaging theory untouched in this paper. One of those immediate research efforts will be the 3D wavefield extrapolation using the Gabor imaging theory, which is under research, and some in-progress research results, such as impulse response tests, have been shown in another paper in this volume.

## ACKNOWLEDGMENTS

We wish to thank the Consortium of Research in Elastic Wave Exploration Seismology (CREWES) and the sponsors for financial support of this research. Thanks goes to the Pacific Institute of Mathematical Sciences (PIMS), Mathematics of Information Tech-

nology and Complex Systems (MITACS) and the Pseudodifferential Operator Theory in Seismic Imaging (POTSI) for financial support. We thank Chad Hogan and David Heley for their careful reviewing of this paper and giving constructive suggestions. The first author also thanks Canadian Society of Exploration Geophysicists (CSEG) for scholarships (2005-2007) supporting his Ph D thesis research.

## REFERENCES

- Claerbout, J. F., and Doherty, S. M., 1972, Downward continuation of moveout-corrected seismograms: *Geophysics*, **37**, 741–768.
- Ferguson, R. J., and Margrave, G. F., 2002, Prestack depth migration by symmetric nonstationary phase shift: *Geophysics*, **67**, No. 2, 594–603.
- Gazdag, J., 1978, Wave equation migration with the phase-shift method: *Geophysics*, **43**, No. 7, 1342–1351.
- Gazdag, J., and Sguazzero, P., 1984, Migration of seismic data by phase shift plus interpolation: *Geophysics*, **49**, No. 2, 124–131.
- Grossman, J. P., Margrave, G. F., and Lamoureux, M. P., 2002a, Constructing adaptive, nonuniform Gabor frames from partitions of unity: CREWES Research Report, **14**.
- Grossman, J. P., Margrave, G. F., and Lamoureux, M. P., 2002b, Fast wavefield extrapolation by phase-shift in the nonuniform Gabor domain: CREWES Research Report, **14**.
- Jin, S., and Wu, R., 1998, Depth migration using the windowed generalized screen propagators: SEG Expanded Abstracts, **17**, 1843.
- Jin, S., Xu, S., and Mosher, C. C., 2002, Migration with a local phase screen propagator: SEG Expanded Abstracts, **21**, 1164.
- Kosloff, D., and Kessler, D., 1987, Accurate depth migration by a generalized phase-shift method: *Geophysics*, **52**, No. 8, 1074–1084.
- Loewenthal, D., Lu, L., Roberson, R., and Sherwood, J. W. C., 1976, The wave equation applied to migration: *Geophys. Prosp.*, **24**, 380–399.
- Ma, Y., and Margrave, G. F., 2005a, A new adaptive windowing algorithm for the Gabor depth imaging: CREWES Research Report, **17**.
- Ma, Y., and Margrave, G. F., 2005b, Prestack depth migration with the Gabor transform: CREWES Research Report, **17**.
- Ma, Y., and Margrave, G. F., 2006a, Adaptive partitioning for 3D Gabor wavefield extrapolation: CREWES Research Report, **18**.
- Ma, Y., and Margrave, G. F., 2006b, Prestack depth imaging with the Gabor transform: SEG Expanded Abstracts, **25**, 2504–2508.
- Ma, Y., and Margrave, G. F., 2006c, Prestack depth migration with the Gabor transform: CSEG National Conference Abstracts.
- Margrave, G. F., Al-Saleh, S. M., Geiger, H. D., and Lamoureux, M. P., 2004, The FOCI algorithm for seismic depth migration: CREWES Research Report, **16**.
- Margrave, G. F., and Ferguson, R. J., 1999, Wavefield extrapolation by nonstationary phase shift: *Geophysics*, **64**, No. 4, 1067–1078.
- Margrave, G. F., Geiger, H. D., Al-Saleh, S. M., and Lamoureux, M. P., 2006, Improving explicit seismic depth migration with a stabilizing wiener filter and spatial resampling: *Geophysics*, **71**, No. 3, S111–S120.
- Roberts, P., Huang, L., Burch, C., Fehler, M., and Hildebrand, S., 1997, Prestack depth migration for complex 2d structure using phase-screen propagators: SEG Expanded Abstracts, **16**, 1282.
- Rousseau, J., and de Hoop, M. V., 2001, Modeling and imaging with the scalar generalized-screen algorithms in isotropic media: *Geophysics*, **66**, 1551.
- Stoffa, P. L., Fokkema, J. T., de Luna Freire, R. M., and Kessinger, W. P., 1990, Split-step fourier migration: *Geophysics*, **55**, 410–421.
- Wu, R., and Huang, L., 1992, Scattered calculation in heterogeneous media using a phase-screen propagator: SEG Expanded Abstracts, **11**, 1289.